International Journal of Pharmaceutics 668 (2025) 124963

Contents lists available at ScienceDirect

International Journal of Pharmaceutics

journal homepage: www.elsevier.com/locate/ijpharm

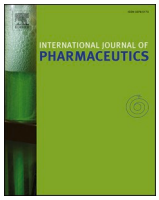

Biodegradable lipid bilayer-assisted Active Ingredient green J- aggregates for photothermal therapy: Formulation, *in vitro* toxicity and *in vivo* clearance

Wafa T. Al-Jamal [a,1,*], Cristian Reboredo [a,1], Ubah Abdi [a], Pia Curci [b], Raghed Qadadeh [a], Hamoud Alotaibi [a,c], Luca Casettari [b], Taher Hatahet [a,d]

[a] School of Pharmacy, Queen's University Belfast, 97 Lisburn Rd, Belfast BT9 7BL, United Kingdom
[b] School of Pharmacy, Department of Biomolecular Sciences, University of Urbino Carlo Bo, Piazza del Rinascimento n°06, 61029 Urbino, PU, Italy
[c] Department of Pharmaceutics, College of Pharmacy, Northern Border University, Arar 91431, Saudi Arabia
[d] China Medical University and Queen's University Joint College, Shenyang, People's Republic of China

ARTICLE INFO

Keywords:
Active Ingredient green J-aggregate
(IJA) Photothermal therapy (PTT)
Liposomes, imaging
IJA clearance
Biodegradable photothermal agent

ABSTRACT

Active Ingredient green (ICG) J-aggregates (IJA) are a unique form of aggregation that exhibits superior properties to monomeric ICG. Despite their higher photoacoustic (PA) signals for imaging and heating stability during pho-tothermal therapy (PTT), they exhibit low stability under a biological milieu. Our group previously proposed a simple procedure for *in-situ* preparation of IJA into liposomes, accelerating their formation and optical proper-ties. To comprehend their potential applications, we systematically investigated the effect of the lipid bilayer composition on ICG J-aggregation and stability. Moreover, their *in vitro* compatibility and photothermal toxicity in monolayers and cancer spheroids, besides their *in vivo* biodistribution and clearance were evaluated. Our findings revealed the importance of high cholesterol and PEG-lipid content and low charged lipids (~ 5 mol %) in liposomes to promote a high IJA/ICG ratio and, thus, high heating stability. More importantly, IJA-liposomes revealed high biocompatibility in monolayer and cancer spheroids with efficient photothermal toxicity. Finally, IJA-liposomes were cleared from the body without toxicity. Interestingly, IJA-liposomes mainly showed lower affinity to the liver than monomeric ICG, resulting in higher renal clearance. Overall, our biodegradable IJA-liposomes could be an excellent alternative to gold-based agents suitable for PA imaging and cancer PTT.

1. Introduction

Photothermal therapy (PTT) is a promising strategy for cancer therapy due to its selectivity, efficacy, minimal invasiveness and side effects (Alamdari et al., 2022, Pucci et al., 2019, Li et al., 2020). Its direct cytotoxic effect on cancer cells has also been successful in activating the immune system to fight cancer (Li et al., 2020). PTT works by converting irradiated light into heat, where the increased temperature (> 45 °C) is sufficient to induce localised cell death and cellular protein denaturation (Fernandes et al., 2020, Pucci et al., 2019, Thirumurugan et al., 2024). Photothermal agents, such as gold-based materials, metal-frame works, and carbon-based constructs, have shown excellent results as photothermal agents. However, their slow degradation and clearance from the body have limited their clinical applications, particularly for systemic administration, highlighting the need for biodegradable alternatives (Thirumurugan et al., 2024).

Active Ingredient green (ICG) is the only near-infrared FDA-approved cyanine dye (Galema et al., 2022, Alander et al., 2012). It is an anionic and water-soluble dye with an absorption and emission peaks of 780 nm and 810–20 nm, respectively. It is used in humans for ophthalmic angiography, determining cardiac output, hepatic function and liver blood flow (Alander et al., 2012). Pre-clinically, ICG has shown prom-ising results in photoacoustic (PA) imaging (Chaudhary et al., 2019) and PTT and photodynamic treatment (PDT) (Yorozu et al., 2022, Hu et al., 2022). However, it presents several shortcomings, such as low photo-thermal and aqueous stability together with a very short blood circu-lation (Alander et al., 2012), which hamper its applications *in vivo*. Encapsulating monomeric ICG into nanocarriers has overcome its optical stabilities and undesirable pharmacokinetics profile (Beziere et al., 2015, Mahmut et al., 2023, Saxena et al., 2004). A slightly different approach was used to tackle its low photothermal stability via J-aggregate formation (Liu et al., 2017, Picchio et al., 2021).

* Corresponding author at: School of Pharmacy, Queen's University Belfast, Belfast BT9 7BL, United Kingdom.
E-mail address: w.al-jamal@qub.ac.uk (W.T. Al-Jamal).
[1] Authors with equal contribution

https://doi.org/10.1016/j.ijpharm.2024.124963
Received 6 July 2024; Received in revised form 8 September 2024; Accepted 15 November 2024
Available online 16 November 2024

ICG is intrinsically capable of forming J-aggregates, a head-to-tail arrangement of the monomers driven by π-π stacking and hydrophobic interactions (Cheung et al., 2020). On the contrary to the monomeric ICG, ICG J-aggregates (IJA) have displayed improved optical stability (Cheung et al., 2020), narrower and bathochromic shifted (~890 nm) absorption spectrum and greater PTT efficacy (Liu et al., 2017, Picchio et al., 2021). It was reported that IJA spontaneously form upon storing ICG at room temperature for several days (Rotermund et al., 1997); however, different approaches have been reported to promote and/or accelerate IJA formation. For instance, high temperature (~65 °C) (Cheung et al., 2020, Liu et al., 2017), increasing dye's concentration (Shakiba et al., 2016), adding salts (Chen et al., 2022), or drugs, such as Active Ingredient (Vincy et al., 2022). Nevertheless, the *in vivo* application of IJA has been limited due to the disruption of the packing in the presence of biological fluids (Farrakhova et al., 2022, Millard et al., 2023, Chan-galvaie et al., 2019, Shakiba et al., 2016). Promisingly, different nano-carriers, such as liposomes (Wood et al., 2021, Cheung et al., 2020), polymeric micelles (Shao et al., 2019) and polymersomes (Changalvaie et al., 2019), have been developed to encapsulate IJA, thus improving its suitability for systemic administration. Nevertheless, these time- consuming procedures ranged from 8 h to 60 days (Wood et al., 2021, Shao et al., 2019).

Our group previously reported a novel and quick approach to developing IJA-templated liposomes using lower concentrations of ICG and milder incubation conditions, where these constructs had comparable photothermal stability to conventional IJA (Cheung et al., 2020). In our former study, using experimental and molecular modelling, we demonstrated the role of the phospholipid length and saturation in promoting IJA formation without affecting their structural integrity, as confirmed with Cryogenic- TEM (Cheung et al., 2020). In the present work, we extend our research to investigate the effect of different formulation parameters, such as cholesterol and PEG-lipid content, lipid surface charge and IJA content on IJA-liposomes' physiochemical properties. More importantly, their stability under physiological conditions, biocompatibility, and PTT in various 2D and 3D cancer models was investigated. Finally, the *in vivo* behaviour in terms of tumour targeting and organ clearance was determined. Overall, the present work provides a better understanding of the formulation parameters needed to prepare optimal photostable IJA-liposomes with promising efficacy and safety profiles suitable for PTT and PA imaging.

2. Materials and methods

2.1. Materials

1,2-Distearoyl-*sn*-glycero-3-phosphocholine (DSPC), 1,2-distearoyl-*sn*-glycero-3-phosphoethanolamine-N-[methoxy(polyethylene glycol)-2000] (DSPE-PEG_{2000}), 1,2-dioleoyloxy-3-trimethylammonium-propane chloride (DOTAP), were generous gifts from Lipoid GmbH (Ludwigshafen, Germany). 1,2-distearoyl-*sn*-glycero-3-phospho-*rac*-glycerol, sodium salt (DSPG) and 1,2-stearoyl-3-trimethylammonium-propane (DSTAP) (chloride salt) were purchased from Avanti Polar Lipids. Cholesterol (Chol), phosphate buffered saline (PBS) tablets, trehalose, hydrochloric acid (HCl) 37 %, absolute ethanol, heat inactivated fetal bovine serum (FBS), resazurin sodium salt, and methylcellulose were purchased from Sigma-Aldrich Ltd. (Dorset, UK). Roswell Park Memorial Institute medium (RPMI), Dulbecco's Modified Eagle Medium (DMEM), 0.05 % trypsin-EDTA phenol red solution, Active Ingredient–Active Ingredient (10,000 U/mL), dimethyl sulfoxide (DMSO) were purchased from Thermo Fisher Scientific. Flat bottom 96-well plates and round bottom 96-well plates were purchased from Sarstedt Ltd (UK). Active Ingredient green (ICG) was purchased from Adooq Bioscience LLC (Irvine, USA). Polycarbonate membranes for liposome extrusion were obtained from Cytiva (Amersham, UK).

2.2. IJA formation

ICG solution was filtered through 0.2 μm membrane filters followed by overnight incubation at 65 °C.

2.3. IJA-liposome preparation and characterisation

2.3.1. Preparation of IJA-liposomes

The ethanolic stock of lipids and ICG were prepared and mixed to prepare liposomes of different lipid compositions (Table 1), as described previously (Cheung et al., 2020). The dried ICG-containing lipid film was hydrated with acidified ultrapure water (pH 3) to achieve a final lipid concentration of 5 mM. ICG concentration in the lipid film ranged from 180- 540 μM. Liposomes were extruded using Avanti manual extruder (Avanti Polar Lipids, Alabaster, USA) or nitrogen Genizer extruder (Genizer LLC, Canada) at 60 °C using different polycarbonate membranes (7 cycles through 0.8 μm (7009482), 11 cycles through 0.2 μm (800281, 10417006) and 15 cycles through 0.1 μm (800309, 110605). Following extrusion, liposomes were annealed for 30 min at 65 °C prior to their purification by size-exclusion chromatography with a PD-10 desalting column (GE Healthcare Life Sciences, Buckinghamshire, UK). Samples were concentrated using a tangential flow filtration (TFF) device (MICROKROS, 300 K, Cat. No. C02-E300-05-N, Repligen, USA).

2.3.2. Physicochemical characterisation of IJA-liposomes

The hydrodynamic diameter, polydispersity and zeta-potential of the freshly prepared samples were measured using dynamic light scattering with the Zetasizer Nano ZS90 (Malvern Panalytical, UK). Prior to the measurement, all the samples were diluted 10 times in DW. Disposable cuvettes (Fisher Scientific, UK) were used for the size and disposable folded capillary cells (Malvern Panalytical, UK) for zeta-potential. At least three runs were performed for each triplicate measurement.

2.3.3. Determination of IJA/ICG and encapsulation efficiencies

IJA optical properties and ICG encapsulation efficiencies (ICG EE) of liposomes were determined by measuring their absorbance using FLUOstar Omega Microplate Reader (BMG Labtech, Buckinghamshire, UK) with a resolution of 1 nm. IJA/ICG absorbance ratio was taken as the ratio of absorbance at 892 nm to 792 nm (i.e. A_{892}/A_{792} ratio). A calibration curve of monomeric ICG (0.3125–10 μM) was established in HBS/DMSO (1/4, v/v) at an absorbance wavelength of 792 nm, corresponding to monomeric ICG. Quantification of loaded ICG was performed by solubilising the purified liposomes in HBS/DMSO (1/4, v/v) and interpolating them using the calibration curve. Based on the initial ICG concentration, serial dilution of the sample was carried out before DMSO solubilising to ensure that the ICG concentration remained within

Table 1
Different liposomal-IJA formulations prepared in this study.

Investigated parameters	Formulations (molar ratio)
Cholesterol effect	DSPC/**Chol**/DSPE-PEG_{2000} (95/**0**/5)
	DSPC/**Chol**/DSPE-PEG_{2000} (95/**10**/5)
	DSPC/**Chol**/DSPE-PEG_{2000} (95/**20**/5)
	DSPC/**Chol**/DSPE-PEG_{2000} (95/**50**/5)
	DSPC/**Chol**/DSPE-PEG_{2000} (95/**100**/5)
DSPE-PEG_{2000} effect	DSPC/Chol/**DSPE-PEG_{2000}** (95/50/**0**)
	DSPC/Chol/**DSPE-PEG_{2000}** (95/50/**2.5**)
	DSPC/Chol/**DSPE-PEG_{2000}** (95/50/**5**)
Charged lipid effect	**DOTAP**/Chol/DSPE-PEG_{2000} (**95**/50/5)
	DSTAP/Chol/DSPE-PEG_{2000} (**95**/50/5)
	DSPG/Chol/DSPE-PEG_{2000} (**95**/50/5)
	DSPC/**DOTAP**/Chol/DSPE-PEG_{2000} (85/**10**/50/5)
	DSPC/**DSTAP**/Chol/DSPE-PEG_{2000} (85/**10**/50/5)
	DSPC/**DOTAP**/Chol/DSPE-PEG_{2000} (90/**5**/50/5)
	DSPC/**DSTAP**/Chol/DSPE-PEG_{2000} (90/**5**/50/5)
	DSPC/**DSPG**/Chol/DSPE-PEG_{2000} (90/**5**/50/5)

the range of our standard curve for correct quantification. ICG EE was determined by taking the ratio between the concentration of encapsulated ICG and the initial ICG concentration.

$$\textit{ICG EE}(\%) = \frac{\textit{Concentration of Encapsulated ICG}}{\textit{Concentration of Initial ICG}} \times 100\%$$

2.3.4. Near-Infrared (NIR laser-induced photothermal heating

The near-infrared (NIR) laser-induced heating capacity of the formulations was assessed by irradiating the samples with a laser at 808 nm and 0.5 W/cm^2, using an FC-808 fibre-coupled laser system (CNI Optoelectronics Tech, Changchun, China). Before the laser irradiation, samples (0.5 mL) were placed in a disposable polystyrene DLS cuvette and warmed up to 35 °C, using a customised holder connected to a water bath via a peristaltic pump (Verderflex, Castleford, UK). Three cycles of irradiation were applied to each sample. The cycles consisted of a 5-minute frame of laser irradiation followed by 5 more minutes of cooling. The temperature of the samples was monitored with a fiber optic thermal probe (Model PRB-G40, Osensa, Canada).

2.3.5. Serum stability evaluation of IJA-liposomes

IJA-liposomes were incubated at 37 °C in PBS, 10 % and 50 % of non-heat inactivated FBS at 37 °C. At different time points, 0.5 mL of the samples were loaded in qEV column (IZON Science Europe Ltd.) and eluted with 0.5 mL of PBS to remove the free IJA and FBS proteins followed by the assessment of IJA-liposomes' physiochemical properties, EE, and IJA ratio, as described previously.

2.3.6. IJA-liposomes lyophilisation

The IJA-lipid film was hydrated with trehalose (pH 3) solution or formed IJA-liposomes were mixed with trehalose solution at different lipid:trehalose molar ratios. All samples were lyophilised for 48 h using in a freeze dryer (Edwards Modulyo F101-01-0000).

2.4. In vitro testing studies

2.4.1. Cell lines and culture conditions

Murine B16-F10 melanoma, murine Panc02 pancreatic, and murine RAW 264.7 macrophage cell lines were obtained from ATCC (USA) and cultured in RPMI 1640 medium, supplemented with 10 % FBS and 1 % Active Ingredient/Active Ingredient. imPSC (immortalised mouse pancreatic stellate cells) were kindly provided by Professor Angela Mathison (Medical College Wisconsin, USA) and cultured in DMEM medium, supplemented with 10 % FBS and 1 % Active Ingredient/Active Ingredient.

All cell lines were cultured in 75 cm^2 flasks (Thermo Fisher Scientific, UK) in a humidified atmosphere at 37 °C and 5 % CO_2. Cell passages were carried out when an 80 % confluency was achieved. For that purpose, solutions containing 0.05 % trypsin for B16-F10, Panc02 and imPSC cell lines and a cell scrapper for the RAW 264.7 cells were used. In addition, *Mycoplasma* spp. contamination tests were routinely carried out.

2.4.2. Cell viability in monolayers

Cells were seeded overnight in a 96-well plate at a density of 1.5 X10^4 cells/well. The next day, the medium was removed, and cells were incubated with 200 μL of different ICG and IJA concentrations (20 – 200 μM) prepared in a cell culture medium. At various time points (24 or 48 h), the treatments were removed, and cells were washed with PBS and supplemented with 200 μL of a resazurin solution (0.01 mg/mL) in a cell culture medium. 4 h post-incubation, 150 μL of supernatants were transferred to a black 96-well plate (Thermo Fisher Scientific, UK). The fluorescence of the transformed resorufin was measured using a BMG plate reader (540/590 nm; ex/em filters). Negative and positive controls of medium and 10 % DMSO solution, respectively, were used. All values were blank (resazurin in medium) corrected, and cell viability was expressed as the percentage between treated and untreated cells.

2.4.3. In vitro PTT therapy in monolayers

Panc02 or imPSC cells were seeded overnight into flat bottom 96-well plates at a density of 1.5 X10^4 cells/well. Next day, treatments were added and incubated with two ICG or IJA concentrations (40 and 100 μM) for 24 more hours. After the incubation period, treatments were removed, and cells were washed with PBS. Each individual well was irradiated with an 808 nm laser for 3 min from a 5 cm distance and achieved a final dose of 2 W/cm^2. During irradiation, the well plate was placed on a heating plate set to 37 °C. After irradiation, cells were washed with PBS prior to the addition of the resazurin solution. The determination of the cell viability was performed, as described above.

2.4.4. Spheroid formation

Cell suspensions containing 7.5 × 10^3 cell/mL in cell culture media containing 20 % methylcellulose (MC) were prepared (supplemented with RPMI 1640 (Panc02 cells) or DMEM (mPSC cells). 200 μL of the cell suspension were added to each well of a round-bottom 96-well plate, leading to a cell density of 1.5X10^3 cells/well. Co-cultured spheroids of imPSC and Panc02 cells (2:1 ratio) were also prepared. Cells were incubated for 3 days to enable spheroid formation. For that purpose, a cell suspension consisting of 5X10^3 cells/mL (imPSC) and 2.5X10^3 cells/mL (Panc02) was prepared in fully supplemented DMEM media containing 20 % MC. Finally, 200 μL of the cell suspension was placed in the wells and allowed to grow. Spheroid pictures were captured using an Olympus CKX41 inverted microscope (Evident Corporation, Tokyo, Japan), coupled to a Qimaging micropublisher 3.3 RTV real-time viewing camera operated using the Qcapture Pro 7 software. Spheroids' size was determined over time using, a Cell3iMager neo (SCREEN holding co. Ltd., Kyoto, Japan) and the results were presented as a percentage of the size of the spheroids on day 3.

2.4.5. Cytotoxicity evaluation of the formulations in spheroids

Spheroids (Panc02, imPSC or Panc02/imPSC) of 500 μm diameter were obtained 3 days post seeding. At that stage, 100 μL medium was removed from each well and replenished with fresh medium containing the relevant treatment to achieve a final ICG or IJA concentration of 40 or 100 μM. Spheroids were incubated with the treatments for 48 h, then, the treatments were removed gradually using five washing of 100 μL fresh medium. Spheroids were allowed to develop for 5 more days, where the medium was replenished every two days, as described earlier. The spheroid's growth was monitored at determined timeframes and represented as a percentage of the size of the spheroids on day 3.

2.4.6. In vitro PTT therapy in spheroids

Panc02/imPSC spheroids were treated as described above. 24 h post incubation, treatments were removed, as described earlier, and each well was irradiated with the 808 nm laser for 5 min, from 5 cm distance and achieve a final dose of 2 W/cm^2. After the irradiation cycle, the cell medium was refreshed to remove any potential cell debris, and spheroids were maintained in the incubator. The spheroid's growth was monitored and represented as a percentage of the size of the spheroids on day 3.

2.5. In vivo testing studies

2.5.1. Animals and tumour models

All animal procedures were performed in compliance with the UK Home Office Code of Practice for the Housing and Care of Animals used in Scientific Procedures. 5–6 week C57BL6 mice (Envigo) were placed on Teklad Global 2019X for 5 days prior to any injection.

Mice' legs were inoculated subcutaneously with 50 μL of Panc02: imPSC (1x10^6: 1x10^6 cells) in PBS using 27 G hypodermic needles. Tumour growth was monitored three times a week using an electronic calliper, and tumour volume was calculated using $V = L*W^2/2$ (V: tumour volume, L: the longest diameter, W: the diameter perpendicular to the length). Biodistribution studies were performed when the tumour

volume reached ~ 200 mm^3.

2.5.2. In vivo biodistribution studies

C57BL6 mice were injected via the tail vein with 40 μg of free ICG, IJA or IJA-DSPC liposomes and fluorescence was visualised immediately, 3 and 24 h post i.v. injection. Fluorescence was detected using In-Vitro Xtreme II (Bruker, USA; excitation 760 nm, emission 860 nm). In separate groups, mice were sacrificed at (1 h, 24 h and 7 days) to quantify the fluorescence intensity in different organs and tissues. Images were quantitatively analysed by drawing regions of interest (ROI) around the tumour region and tissues using Molecular Imaging software MI 7.5 (Bruker, USA). After 7 days, organs were isolated and immediately fixed in 10 % neutral buffer formalin. Tissues were then paraffin-embedded and sectioned for haematoxylin and eosin stains (H&E) according to standard histological protocols at the Royal Veterinary College (London, UK).

2.6. Statistical analysis

Prior to the statistical analyses, the mean, standard deviation, and normality distribution of all the data sets were calculated. The comparisons between groups were performed using a one-way ANOVA followed by a multiple comparison test (Tukey-Kramer). For repeated measurements (e.g., spheroid growth with treatments) a one-way ANOVA for repeated measurements was used. All the calculations were carried out using GraphPad Prism v6 (GraphPad Software, San Diego, CA, USA). Statistical differences are represented as follows: *: $p < 0.05$; **: $p < 0.01$; ***: $p < 0.001$. Figures were plotted using the Origin 8 software (OriginLab Corp, Northampton, MA, USA).

3. Results

3.1. High cholesterol content promotes IJA formation in rigid DSPC:Chol:DSPE-PEG_{2000} liposomes despite decreasing ICG encapsulation efficiency

Table 2 summaries the influence of the Chol content on the physicochemical properties of the formed IJA-liposomes. Interestingly, increasing the Chol:lipid molar ratio led to a significant increase in the liposome size, accompanied by a decrease in the PDI. In addition, the higher Chol ratio significantly improved the IJA/ICG ratio despite the significant reduction in the ICG encapsulation efficiency (EE%). The results of the heating capacities of the formulations are displayed in Fig. 1**A.** Our results showed that liposomes containing Chol higher than 50 mol% displayed the best heating capacity over three cycles of laser irradiation, which was similar to that achieved by free IJA. Moreover, IJA-liposomes containing more than 20 mol% Chol were stable when stored at room temperature for 30 days. On the other hand, liposomes containing less than 20 mol% Chol showed a significant increase in size, PDI, IJA/ICG ratio, highlighting the role that Chol plays in improving IJA formation and the overall stability of formulation during storage (**Fig. S1**).

Table 2
Physicochemical properties of IJA-loaded liposomes containing different cholesterol: lipid molar ratios. Data expressed as the mean ± SD (n = 3). *: $p < 0.05$; **: $p < 0.01$; ***: $p < 0.001$ compared to liposomes without cholesterol.

Liposome composition (molar ratio)	Hydrodynamic diameter (nm)	PDI	IJA/ICG	EE (%)
DSPC/Chol/DSPE-PEG_{2000} (95/0/5)	78.7 ± 5.7	0.21 ± 0.02	2.34 ± 0.92	54.66 ± 5.00
DSPC/Chol/DSPE-PEG_{2000} (95/10/5)	120.4 ± 11.7 ***	0.13 ± 0.04 **	2.94 ± 0.56	44.75 ± 8.04
DSPC/Chol/DSPE-PEG_{2000} (95/20/5)	133.6 ± 3.6 ***	0.08 ± 0.01 ***	4.11 ± 0.19 *	41.61 ± 2.10 *
DSPC/Chol/DSPE-PEG_{2000} (95/50/5)	136.6 ± 3.1 ***	0.04 ± 0.01 ***	4.89 ± 0.14 ***	36.6 ± 3.19 **
DSPC/Chol/DSPE-PEG_{2000} (95/100/5)	135.6 ± 5.0 ***	0.05 ± 0.01 ***	4.67 ± 0.30 **	34.49 ± 2.29 **

3.2. PEGylated lipid increases ICG encapsulation efficiency and IJA/ICG ratio into rigid DSPC:Chol:DSPE-PEG_{2000} liposomes

Table 3 depicts the influence of DSPE-PEG_{2000} content on the properties of IJA-DSPC of liposomes. Interestingly, the presence of pegylated lipid impacted liposomes' size or PDI of the formulations; however, it significantly increased the IJA/ICG ratio and the EE%, compared to non-PEGylated liposomes. No differences were found between liposomes containing 2.5 or 5 mol % DSPE-PEG_{2000}. Fig. 1**B** shows the heating capacity of the IJA-DSPC liposomes with different DSPE-PEG_{2000} content following multiple cycles of laser irradiation. Promisingly, the three formulations displayed the same temperature-raising capacity, comparable to the free IJA.

3.3. Incorporating 5 mol% of positively and negatively charged lipids does not affect IJA-liposomes properties or heating capacity

Next, we explored the possibility of preparing IJA-liposomes with different surface charges. The main physicochemical properties of successfully prepared IJA-liposomes are summarised in Table 4. Surprisingly, the complete replacement of the zwitterionic lipid with positively or negatively charged lipids hindered IJA formation (**Table S1**), while introducing 10 mol% of the charged lipid reduced IJA/ICG ratio and was challenging to extrude (**Table S1**). Liposomes containing 5 mol % of positively charged lipids (i.e., DOTAP and DSTAP) displayed a slight decrease in their surface charge, IJA/ICG ratio and EE%. On the other hand, when liposomes contained 5 mol % of the negatively charged lipid DSPG, a slight increase in their negative surface z-potential was observed. Despite the IJA/ICG ratio not being affected, the EE% was 30–40 % lower than zwitterionic DSPC liposomes. Therefore, 5 mol% of the charged lipid was the optimal amount to include in the IJA-liposomal formulations. These findings indicate that highly positively and negatively charged IJA-liposomes could not be formulated using our presented approach. Promisingly, all IJA-liposomal formulations (IJA-DOTAP, IJA-DSTAP and IJA-DSPG) showed comparable heating capacity to the DSPC-based IJA (Fig. 1**C**).

3.4. IJA-liposomes are stable under physiological conditions and lyophilisation

Our IJA-DSPC and IJA-DOTAP formulations were selected to assess their stability at 37 °C in PBS, 10 % and 50 % FBS. Interestingly, all formulations showed stable size under these conditions, PDI and IJA/ICG ratios up to 24 h (**Table S2**).

Next, two approaches were investigated to optimise the IJA-DSPC lyophilisation for long-term storage, either by hydrating lipid film with different concentrations of trehalose or mixing the latter with preformed IJA-DSPC (**Fig. S2**). The range of lipid to trehalose varied from 1:5–1:20 M ratio. All IJA-liposomes hydrated with different sugar concentrations exhibited comparable physicochemical properties and ICG EE% and IJA/ICG ratio; however, following freeze drying, the size and PDI of IJA-DSPC significantly increased for all the formulations except for the sample hydrated with the highest sugar content 1:20 ratio (**Fig. S2A**). Using the highest sugar content, the zeta potential of 1:20 ratio also increased to −30 mV, and the highest EE% and IJA/ICG were maintained.

On the contrary, mixing preformed IJA-DPSC with lower amount of trehalose concentrations significantly increased liposome hydrodynamic size and PDI (**Fig. S2B**). Interestingly, at 1:20 ratio, the IJA-DSPC size and PDI remained unchanged after freeze drying, with minimal change in the surface charge. Furthermore, the highest ratio of 1:20

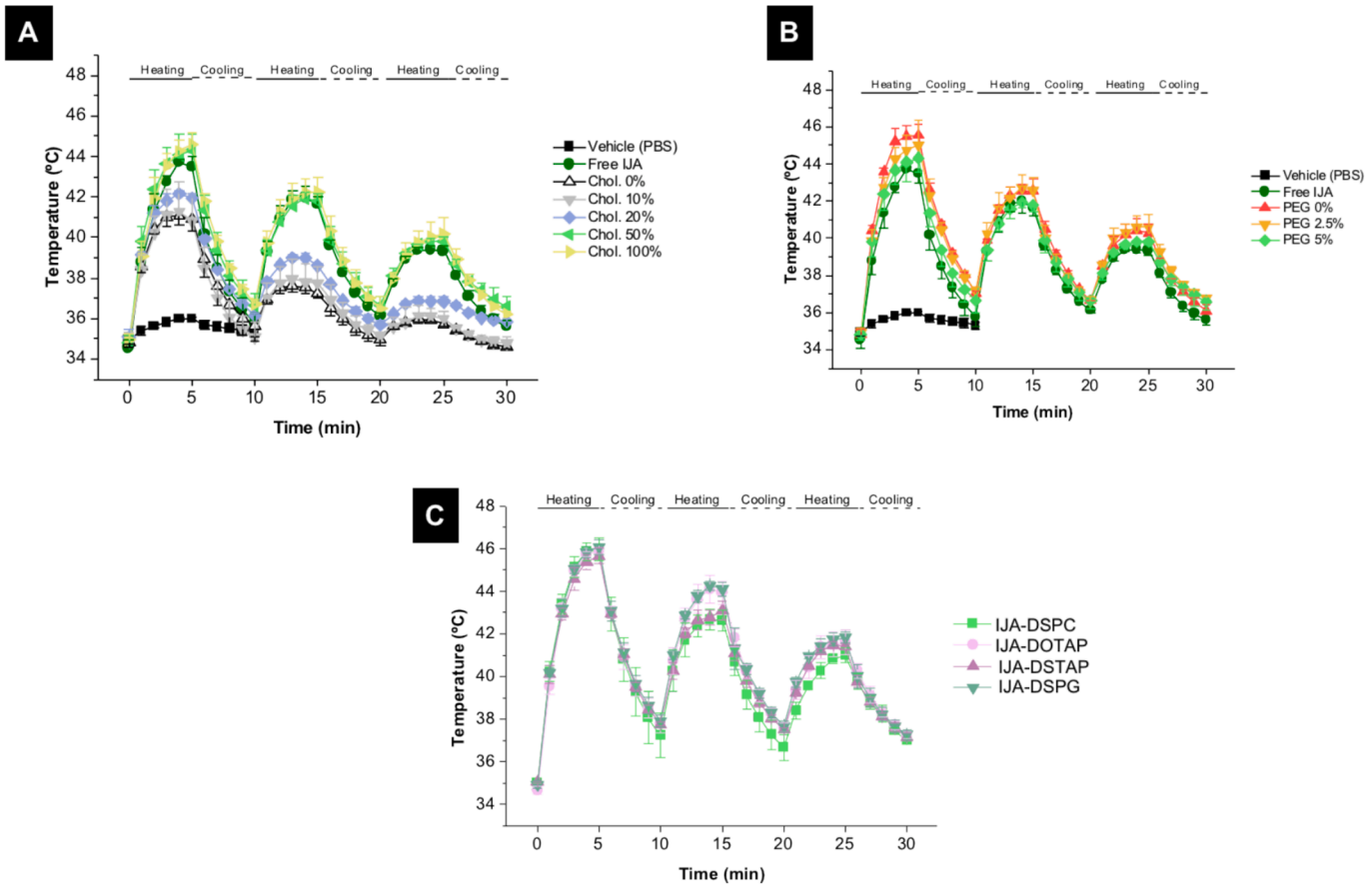

Fig. 1. Heating capacity of IJA-loaded liposomes containing varying molar ratios of (A) Chol, (B) DSPE-PEG_{2000} (PEG), and (C) 5 mol % of positively and negatively charged lipid during 3 cycles of 5 min irradiation. For all the formulations, the IJA concentration was 12.9 μM. Data represented as the mean ± SD (n = 3).

Table 3
Physicochemical properties of IJA-loaded liposomes containing varying molar ratios of DSPE-PEG_{2000}. Data expressed as the mean ± SD (n = 3). **: $p < 0.01$; ***: $p < 0.001$ compared to liposomes without DSPE-PEG_{2000}.

Liposome composition (molar ratio)	Hydrodynamic diameter (nm)	PDI	IJA/ICG	EE (%)
DSPC/Chol/DSPE-PEG_{2000} (95/50/0)	139.1 ± 2.7	0.05 ± 0.01	3.75 ± 0.14	15.52 ± 6.10
DSPC/Chol/DSPE-PEG_{2000} (95/50/2.5)	139.8 ± 11.2	0.04 ± 0.01	4.85 ± 0.01 ***	34.97 ± 3.94 **
DSPC/Chol/DSPE-PEG_{2000} (95/50/5)	136.6 ± 3.0	0.04 ± 0.01	4.89 ± 0.14 ***	34.28 ± 3.67 **

Table 4
Physicochemical properties of the successfully IJA-loaded liposomes with different lipid compositions. Data expressed as the mean ± SD (n = 3).

Liposome composition (molar ratio)	**Hydrodynamic diameter (nm)**	**PDI**	***ζ-Potential* (mV)**	**IJA/ICG**	**EE (%)**
DSPC/Chol/DSPE-PEG_{2000} (95/50/5)	138.2 ± 1.5	0.04 ± 0.01	−12.6 ± 0.1	4.89 ± 0.14	36.6 ± 3.19
DSPC/DOTAP/Chol/DSPE-PEG_{2000} (90/5/50/5)	140.1 ± 2.3	0.05 ± 0.01	−6.9 ± 0.6	4.34 ± 0.14	26.19 ± 0.74
DSPC/DSTAP/Chol/DSPE-PEG_{2000} (90/5/50/5)	132.2 ± 3.5	0.04 ± 0.01	−9.5 ± 0.7	4.01 ± 0.06	26.30 ± 0.02
DSPC/DSPG/Chol/DSPE-PEG_{2000} (90/5/50/5)	136.7 ± 5.5	0.04 ± 0.01	−15.3 ± 1.0	4.73 ± 0.22	22.19 ± 3.66

maintained the highest ICG and IJA/ICG ratio. The lyophilised IJA-DPSC premixed at 1:20 lipid:trehalose concentration exhibited the same heating capacity as the freshly prepared sample (data not shown), confirming the suitability of the procedure for long-term storage of IJA-DSPC.

3.5. IJA exhibits higher biocompatibility than free ICG in cancerous and non-cancerous cell lines

The biocompatibility of ICG and preformed IJA was assessed in a range of murine cancerous cell lines (B16-F10 and Panc02), fibroblasts (imPSC) and macrophages (RAW264.7) up to 48 h. In both cancer cell lines, ICG (20–100 μM) showed toxicity after 48 h. In some cell lines, reduced toxicity was observed at 200 μM, probably due to ICG aggregation at high concentrations, reducing cellular uptake and toxicity. Promisingly, IJA under equivalent conditions showed significantly higher cell viability and, therefore, safety profile (Fig. 2).

Strikingly, IJA showed higher cell viability than ICG in both non-cancerous cells (fibroblasts and macrophages, except at 200 μM/48 h), suggesting higher *in vitro* compatibility. However, a significant increase (~10–30 %) in cell viability was observed with imPSC incubated with IJA up 48 h, suggesting cell proliferation. Similarly, macrophages

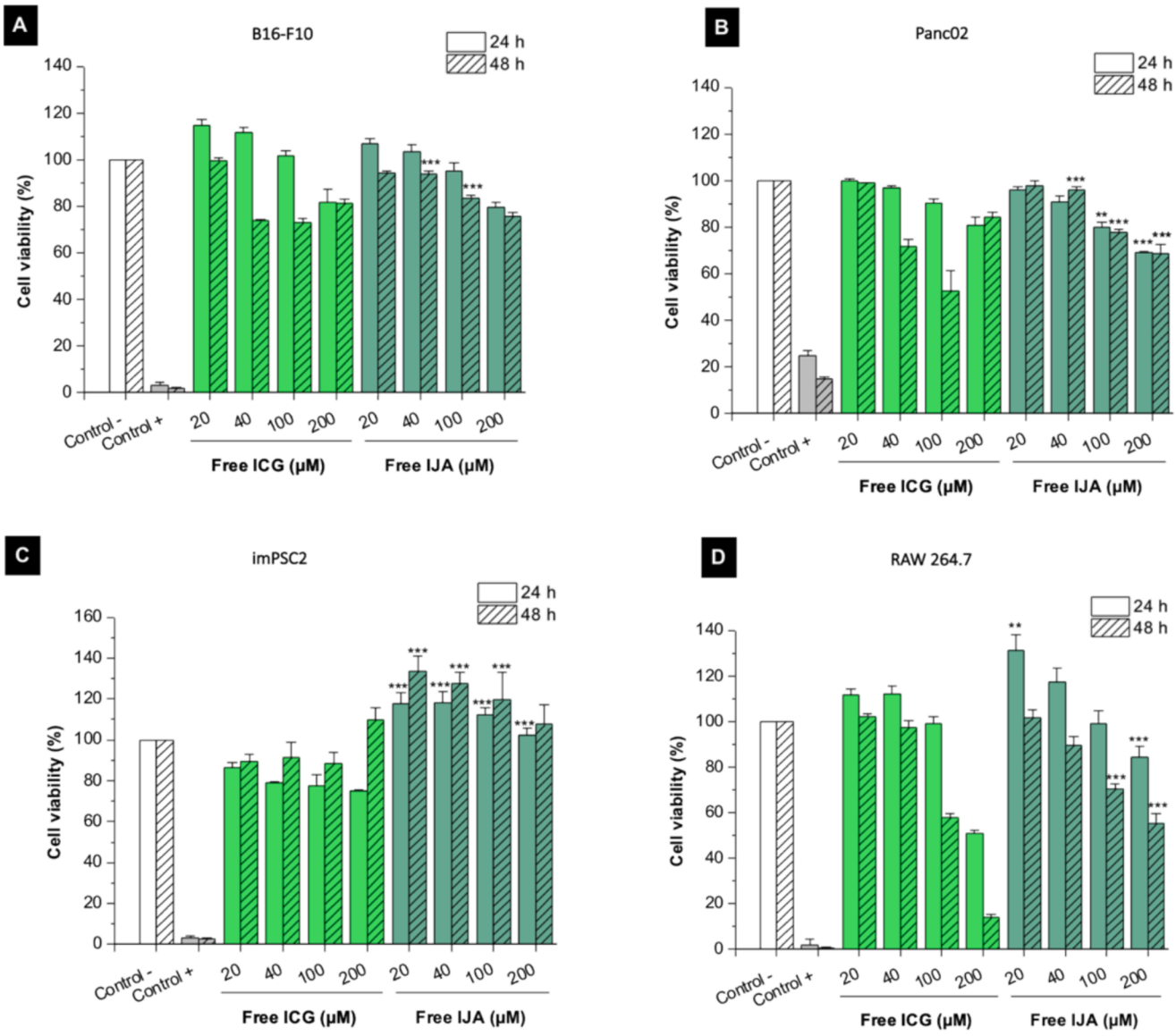

Fig. 2. Cell viability of IJA and ICG in murine cancerous and non-cancerous cell lines. Cell viability was assessed in (A) B16-F10, (B) Panc02, (C) imPSC fibroblasts and (D) RAW 264.7 macrophages using resazurin assay. N = 3 with 6 wells/treatment. Statistical differences are comparing free IJA with ICG at the same concentration and incubation time. **: $p < 0.01$; ***: $p < 0.001$.

incubated with IJA showed a slight increase in cell viability (20–100 μM) at 24 h before further reduction. The mechanism behind this unexpected increase in cell viability requires further investigation, however, our preliminary results suggest oxidative stress in imPSC, as this proliferation was completely inhibited in the presence of 3 mM of GSH antioxidant (Fig. S3).

3.6. IJA-liposomes exhibit efficient PTT activity in cell monolayers

To enable biological testing, 540 μM was the maximal IJA concentration used to load into liposomes without affecting their physicochemical properties (data not shown). The toxicity of the optimal IJA-liposomes; namely, IJA-DSPC, IJA-DOTAP, and IJA-DSPG liposomes were tested in Panc02 and imPSC cells (Fig. 3**A-B**). Interestingly, all IJA-liposomes showed comparable cell viability to free IJA at 40 and 100 μM. A slight but significant cell viability reduction was observed in Panc02 cells. IJA-liposomes exhibited a slight increase in imPSC cell viability, similar to free IJA. Despite its biocompatibility, due to the lack of IJA-DSPG-liposome reproducibility during scale-up, this formulation was not taken forward.

Next, the PTT effect of the different treatments was assessed by incubating cells for 24 h with the different treatments at a concentration of 40 μM IJA, then irradiated for 3 min with an 808 nm wavelength laser. Following laser irradiation, the cell viability was assessed using the resazurin test. Promisingly, upon laser irradiation, a complete loss in cell viability was achieved using 40 μM (Fig. 3**C-D**), suggesting IJA, IJA-DPSC and IJA-DOTAP as efficient PTT agents.

3.7. IJA-liposomes PTT slows down growth in 3D spheroids without promoting their growth, unlike free IJA

Spheroids are three-dimensional (3D) culture models of one or more types of cells that mimic tumours *in vivo*. To assess the PTT efficacy of IJA-liposomes in 3D models, co-culture spheroids of Panc02:imPSC spheroids were cultured and treated with free IJA, IJA-DSPC and IJA-DOTAP liposomes. 10 % DMSO was used as a positive control. Our results showed that none of the IJA-liposomes affected spheroid growth, which was comparable to the control spheroids, highlighting their

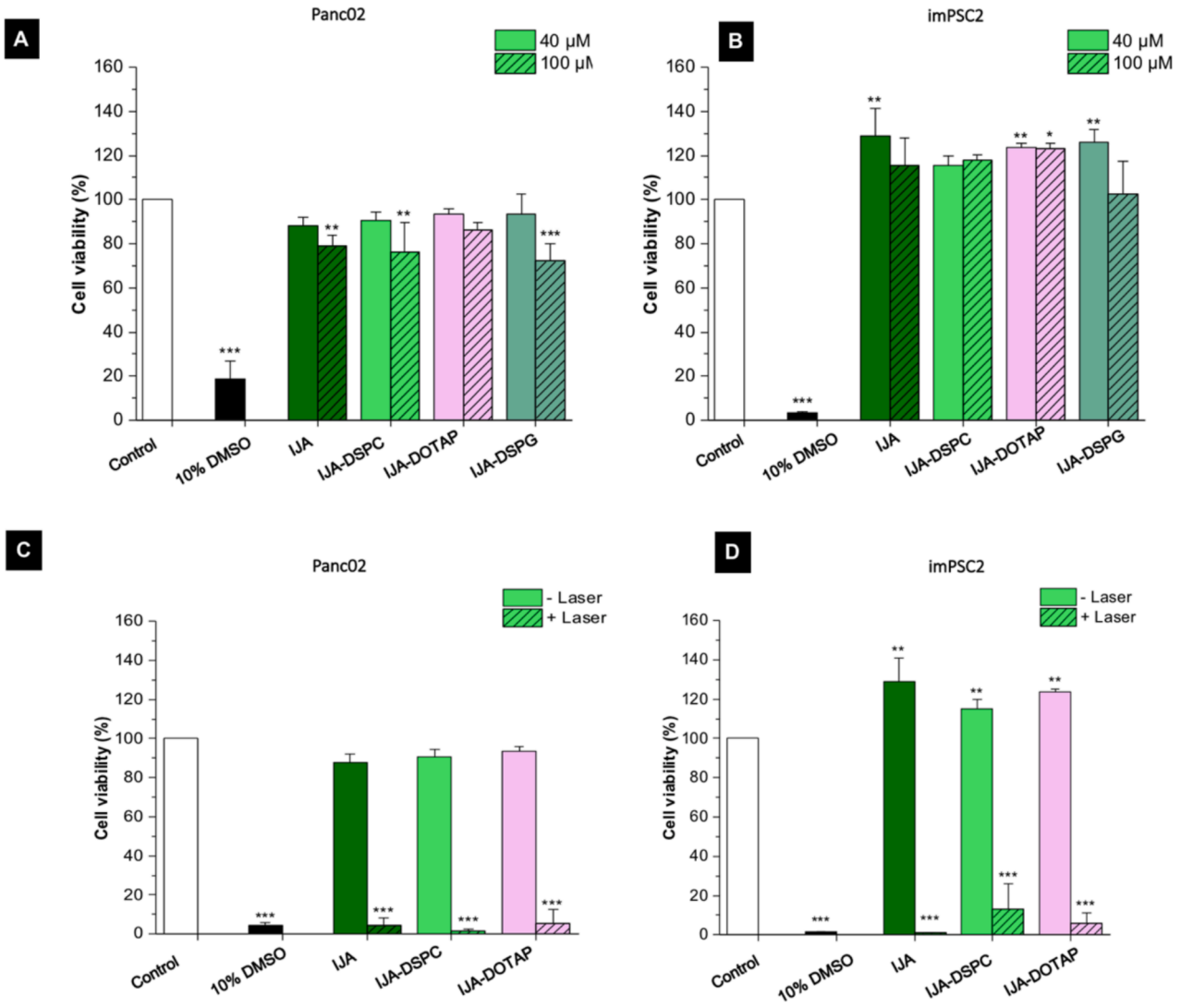

Fig. 3. Cell viability and PTT activity of IJA-liposomes in different cell lines. free IJA or IJA-liposomes for 24 h were incubated with (A) cancerous Panc02 and (B) imPSC fibroblast cell lines. (C) Panc02 and (D) imPSC cell cells were incubated with 40 μM of different IJA-liposomes for 24 h, then washed and irradiated with 808 nm laser (3 min, 2 W/cm^2). Cell viability was assessed using resazurin assay. 10 % DMSO was used as a positive control. N = 3 with 6 wells/treatment. Statistical differences were compared to untreated control. *: $p < 0.05$; **: $p < 0.01$; ***: $p < 0.001$.

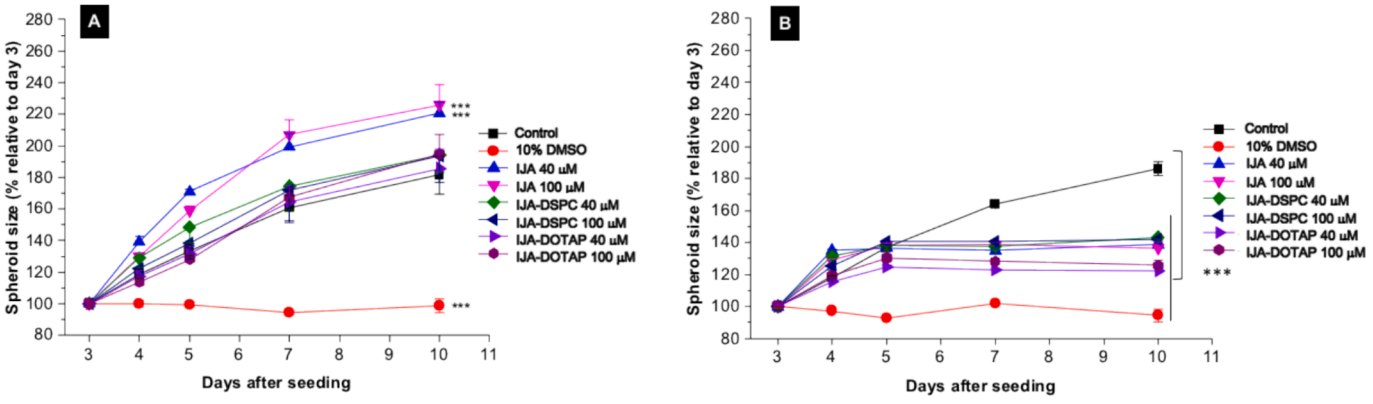

Fig. 4. Cell viability and PTT activity of IJA-liposomes in Panc02:imPSC spheroids. All spheroids were treated on day 3 of spheroid seeding with IJA, IJA-DSPC or IJA-DOTAP for 24 h. After that the treatment was removed and left (A) unirradiated or (B) irradiated with 808 nm laser for 5 min (2 W/cm^2). The spheroid size was monitored and the results were expressed as % increase relative to spheroid volume on day 3 (n = 3; experiments with 4 wells/treatment). *** $p < 0.001$ compared to the control group.

biocompatibility (Fig. 4**A**). Surprisingly, IJA at both concentrations enhanced spheroid growth, as previously observed with imPSC monolayer (Fig. 2**C**). Interestingly, this effect was eliminated with both IJA-liposomes. In separate experiments, it was noted that the same concentrations of IJA promoted spheroid growth in imPSC spheroids and Panc02:imPSC spheroids (**Fig. S4 & S5)** but not in Panc02 spheroids (**Fig. S6**). Also, the high concentration of ICG showed significant toxicity, as indicated by a smaller spheroid size (**Fig S4-S6**). Overall, our IJA-liposomes showed higher compatibility compared to IJA and ICG. This enhanced proliferation in imPSC-containing spheroids could be attributed to higher oxidative stress, which requires further investigation.

Promisingly, upon 808 nm laser irradiation, all IJA-treated spheroids exhibited growth inhibition compared to the untreated spheroids, confirming the efficacy of IJA and both IJA-liposomes as PTT agents against cancer (Fig. 4**B**). No significant difference was seen between the three groups. Nevertheless, IJA-liposomes did not promote proliferation in non-irradiated cells.

3.8. IJA-liposomes accumulate in tumours and are excreted through the liver and kidneys following intravenous administration

To evaluate IJA-DSPC behavior *in vivo,* 40 μg of free ICG, IJA or IJA-DSPC liposomes were injected intravenously in Panc02/imPSC-tumour-bearing mice and monitored their biodistribution and tumour targeting for 1 and 24 h using live imaging. For clearance, the same dose was injected in healthy mice and kept for 7 days. It is important to note that the significant differences in the fluorescence intensity of ICG and IJA, IJA-liposomes (**Fig. S7**) made the direct comparison difficult between groups. Therefore, it was more accurate to monitor the signal changes over time for each group. Fig. 5 contrasts the biodistribution of ICG, IJA and IJA-liposomes in tumour-bearing mice following intravenous administration. It was clear that ICG exhibited rapid liver accumulation (1 h), which significantly decreased over 24 h, due to hepatic clearance of ICG. It also showed visible signals in the tumour (side view, white arrows) implanted on the lower leg. A similar clearance profile was observed in the IJA and IJA-DSPC liposomes, confirming their evident tumour accumulation and rapid body clearance. The lower abdominal signals in the IJA-DSPC group could be due to the high serum stability and longer blood circulation of PEGylated liposomes, reducing their liver uptake following systemic administration (Al-Jamal et al., 2012). Tumour accumulation was evident in all groups at 1 and 24 h, as shown in *ex vivo* tumours (Fig. 5).

Upon *ex vivo* imaging of all organs isolated from mice, it was evident that free ICG had the highest accumulation in the liver up to 7 days, with a significant reduction over time (Fig. 6**A & B**). Unexpectedly, 7 days post-injection, ICG signals were still present, and the liver exhibited the highest signals of all other organs, followed by the spleen and kidney (Fig. 6). Such findings have not been reported earlier since 48 h was the longest duration declared in the literature for ICG pharmacokinetics (Wang et al., 2022). On the contrary, between 1–7 days, the kidneys showed the high signals in the mice injected with IJA and IJA-DSPC, which was higher or comprable to the liver , indicating the significant role of the kidneys in IJA and IJA-DSPC clearance (Fig. 6A). This finding was in agreement with other reports indicating that altering ICG by PEGylation of loading into liposomes changes its affinity to the liver due to its reduced binding to the HSA protein in the blood (Friedman-Levi et al., 2018). It is worth mentioning that quantifying ICG or IJA in collected samples (blood or organs) using HPLC was not possible using both fluorescence or UV detectors due to low ICG stability in biological samples, which is in agreement with others (Ott et al., 1993, Mindt et al., 2018).

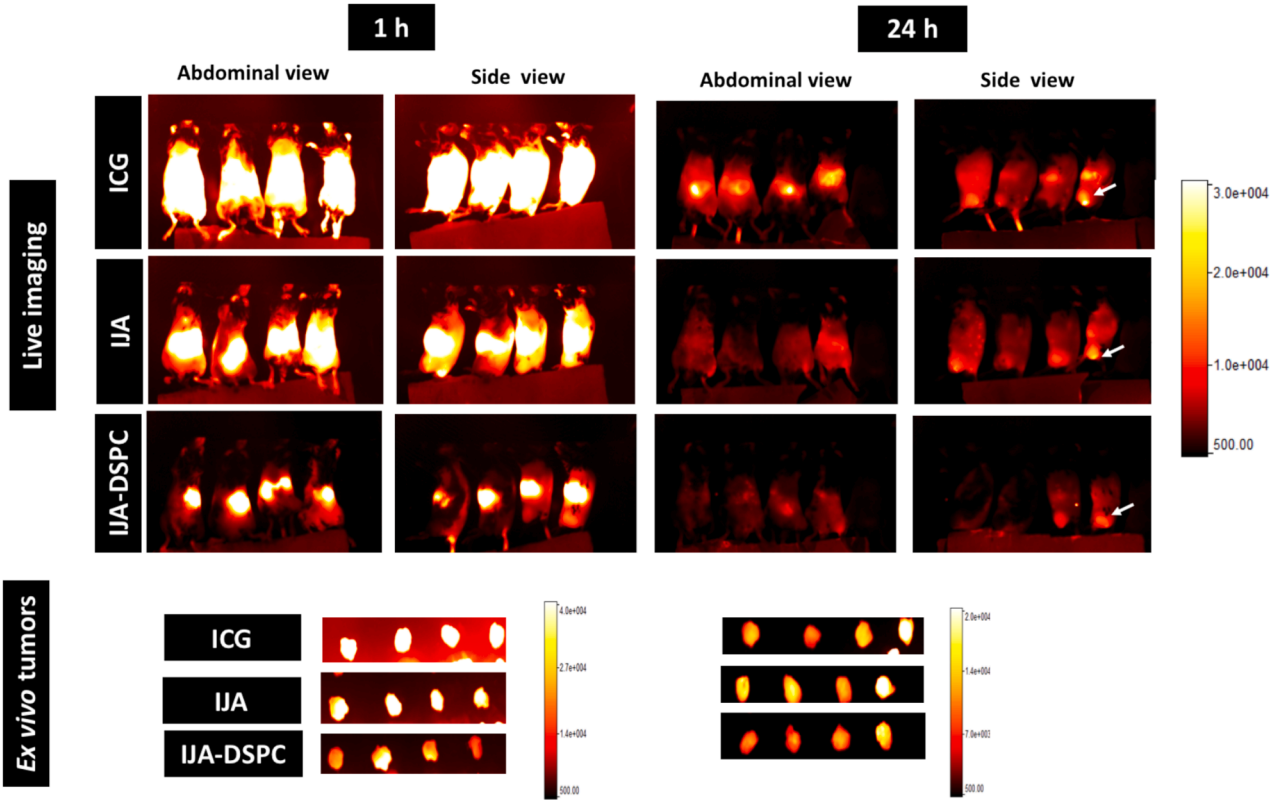

Fig. 5. Live and *ex vivo* fluorescence imaging of IJA-DSPC liposomes biodistribution in Panc02:imPSC-tumour-bearing mice following intravenous administration. A total of 40 μg of ICG, IJA or IJA-DSPC was injected intravenously and imaged with the Bruker at 1 and 24 h. The side view illustrated ICG or IJA tumour accumulation in mice (as indicated by the white arrows) inoculated at the lower part of the leg (n = 4). *Ex vivo* tumours were presented using two different fluorescence scales.

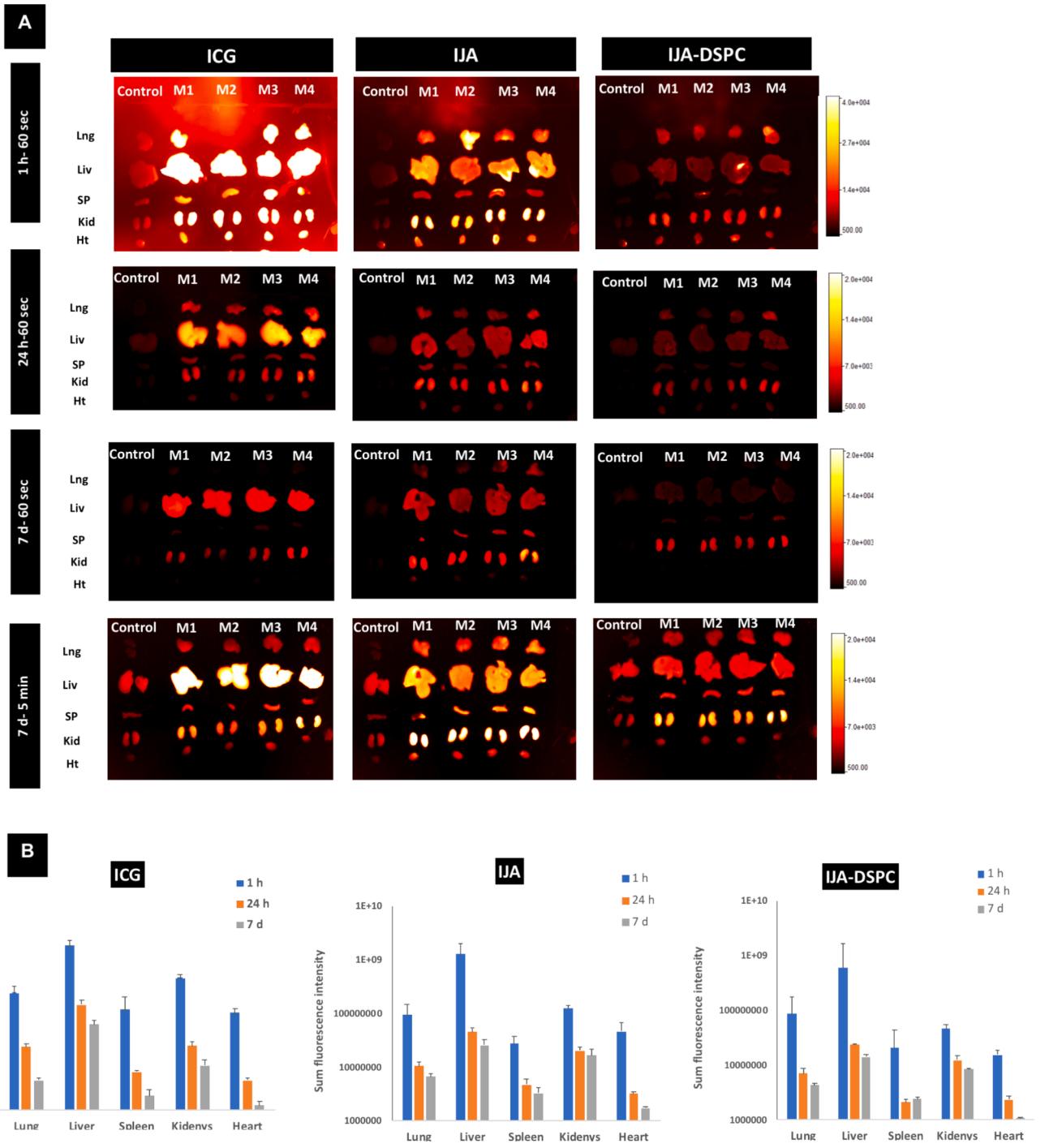

Fig. 6. ***Ex vivo*** **imaging of IJA-DPSC liposome organ biodistribution in C57BL6 mice post intravenous administration.** (A) Organs from mice injected with 40 μg ICG, IJA or IJA-DSPC were isolated and imaged with 20-second exposure time with an additional 5 min exposed for the 7 d samples. Organ abbreviations: Lng: lung, Liv: liver, Sp: spleen, Kid: kidneys, Ht: heart. (B) The fluorescence intensity in these organs was quantified using the Bruker software and plotted as a sum of fluorescence intensity (n = 4 mice per group).

Overall, free ICG and IJA formulations showed significant clearance from the body over time. Despite the remaining dye present in the body for up to 7 days, the findings indicate that good clearance requires more time. Promsingly, no histological changes were observed in all organs examined after 7 days of administering the different treatments (Fig. 7). However, further work is warranted to ensure the time required for the complete clearance of IJA-DSPC. Moreover, extensive safety analysis will be carried out, such as histological examinations and blood tests for liver and kidney functions.

4. Discussion

Cancer thermal therapy has attracted much attention in cancer management due to its high selectivity, efficiency, and safety. Near-infrared (NIR) photothermal absorbers have advanced PTT, conferring a deeper light penetration (Alamdari et al., 2022, Pucci et al., 2019, Li et al., 2020). Inorganic photothermal agents, such as gold, magnetic, and carbon-based nanoparticles, have extraordinary stability upon multiple NIR irradiation. However, several concerns regarding their

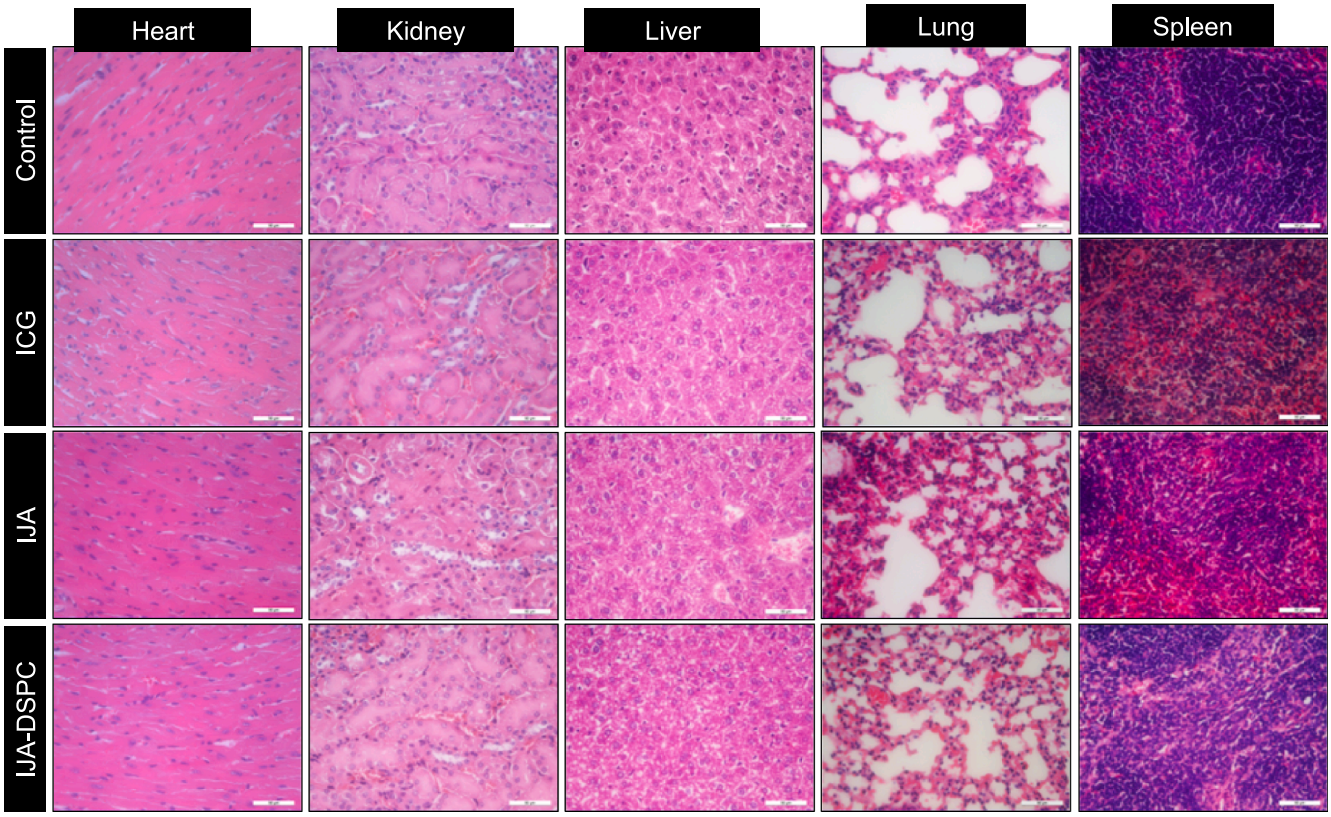

Fig. 7. Histological examination of mice organs injected intravenously with 40 μg ICG, IJA and IJA-DSPC liposomes. H&E staining of heart, kidney, liver, lung, and spleen tissues from C57BL6 mice after 7 days of injection. Magnification 40x, scale bar = 50 μm.

clearance and long-term safety have hindered their clinical translation, particularly for systemic administration (Thirumurugan et al., 2024).

ICG is the only NIR cyanine dye approved by the FDA for optical imaging (Galema et al., 2022, Alander et al., 2012). Promisingly, J-aggregation of ICG confers superior properties compared to the monomeric ICG, thus promising agents for PTT and PA imaging (Liu et al., 2017, Shakiba et al., 2016, Wood et al., 2021). IJA were initially prepared by incubating high concentrations of ICG at 65 °C for 24 h (Cheung et al., 2020, Liu et al., 2017). Moreover, ICG aggregation has been promoted using acid pH, divalent cations, multivalent ions and drugs (Shao et al., 2019, Chen et al., 2022, Lin et al., 2021, Vincy et al., 2022). Despite the diversity of IJA preparation methods, they are considered time-consuming (Wood et al., 2021, Shao et al., 2019) and result in unstable IJA in biological media (Farrakhova et al., 2022, Millard et al., 2023, Changalvaie et al., 2019, Shakiba et al., 2016). To overcome the latter shortcoming, IJA has been successfully loaded into liposomes (Cheung et al., 2020, Wood et al., 2021), micelles (Shao et al., 2019) and polymersomes (Changalvaie et al., 2019).

To date, there is only one study of liposomal IJA for PA imaging. That study encapsulated the monomeric ICG into the aqueous core of rigid liposomes and left them for 60 days at 40 °C (Wood et al., 2021) to promote IJA formation into liposomes. Previously, our group described *in-situ* IJA-loaded liposomes using low ICG concentrations and short preparation time (~2h) (Cheung et al., 2020). In the current work, we extend our previous investigation to optimise IJA formation into a rigid lipid bilayer by varying the cholesterol content, DSPE-PEG_{2000} molar ratio, and lipid charge. Moreover, we intended to improve the IJA/ICG ratio by using an acidic hydration medium (pH 3), as suggested by others reporting that the preparation of polymersomes at an acidic pH improved the IJA/ICG ratios in the formulation (Changalvaie et al., 2019). Similarly, Shao and coworkers reported that acidic pH promoted ICG aggregation into polymeric DSPE-PEG_{2000}-NH_2 micelles (Shao et al., 2019). Promisingly, our developed IJA-liposomes were not only reproducible and quick to prepare, but they showed superior stability in biological conditions and following lyophilisation **(Table S2, Fig. S2).**

Cholesterol is known to increase the packing of phospholipids (Marquardt et al., 2016, Nakhaei et al., 2021) thus promoting IJA formation into liposomes. Our findings confirmed that increasing the molar ratio of cholesterol in the formulations led to a significant improvement in the liposomes' hydrodynamic diameter, PDI, long-term stability and IJA/ICG ratios, resulting in improved heating capacity (Table 1, Fig. 1**A**). On the contrary, increasing the cholesterol content reduced the ICG EE%, which could be attributed to a competitive accommodation of Chol (Nakhaei et al., 2021) and ICG molecules (Lajunen et al., 2018) within the lipid bilayer. Interestingly, incorporating DSPE-PEG_{2000} into the formulation did not influence the main physicochemical properties of the resulting liposomes. However, its presence increased the IJA/ICG ratio and the EE% (Table 2). This finding is in agreement with our previous dynamic modelling studies, which reported ICG aggregation in the IJA between the external surface of rigid liposomes and the surface PEG chains (Cheung et al., 2020). Finally, exceeding 5 mol% of the charged lipids decreased the IJA/ICG ratio and ICG EE% (**Table S1**), which could be due to the interaction of the headgroups with the ICG, hindering its aggregation in liposomes. Hence, liposomes composed mainly of zwitterionic lipids (i.e., DSPC) displayed the optimal properties (Table 3). This phenomenon was previously observed for other cyanine dyes, where zwitterionic lipids were the best template for J-aggregate formation (Mo and Yip, 2009).

Despite the well-known safety of ICG *in vitro* and *in vivo* (Alander et al., 2012, Alford et al., 2009), there are scarce resources about IJA safety *in vitro* or *in vivo*. Millard *et. al.* compared the safety and cellular uptake of free IJA and ICG to self-assembled IJA-calixarenes nanoparticles and reported higher toxicity of IJA in FaDu human head and neck squamous carcinoma cells than the IJA nanoparticles or free ICG (Millard et al., 2023). Liu *et. al.* reported comparable toxicity of IJA and ICG into the HUVEC cell line however, at higher concentrations, IJA

showed some cytotoxicity to 4T1 cancer cells (Liu et al., 2017). In our work, IJA displayed comparable or lower cytotoxicity than ICG, depending on the cell line. Surprisingly, free IJA promoted growth in non-cancerous cell lines, such as imPSC and RAW 264.7 cells (Figs. 2 & 4). This proliferative-enhancing effect was more evident at lower IJA concentrations, probably because of cytotoxicity at higher concentrations. We believe that cell proliferation was mainly attributed to oxidative stress, leading to imPSC proliferation, migration, and increased extracellular matrix (ECM) production (Fu et al., 2018, Jin et al., 2020). This assumption was verified since cell proliferation was eliminated in the presence of the glutathione antioxidant (**Fig. S3**). Similar to monolayers, and unlike ICG, IJA-induced proliferation in imPSC-containing spheroids resulted in larger spheroids with irregular shapes in imPSC:Panc02 spheroids (Fig. S4-5). The irregular shape in the co-cultured spheroids could be attributed to the faster growth of the imPSC compared to the Panc02 cells, resulting in protruding buds on the surface of the spheroids. These unprecedented findings impose some safety concerns about free IJA in non-cancerous cells and in the absence of PTT, such as for PA imaging, which requires further studies.

Promisingly, unlike free IJA, liposomes were safer *in vitro* without laser irradiation (Fig. 4A). Loading IJA into liposomes could reduce or eliminate ROS-triggered activation in imPSC, which requires further investigation. Nevertheless, with 808 nm laser irradiation, both IJA-liposomes were as effective as free IJA in inhibiting cell growth in cancer monolayers and spheroids (Fig. 4**B**). Our results show that IJA-liposomes could be considered a safe and effective PTT agent compared to the free IJA. This finding contradicts Wood *et. al.,* who reported HUVECS cell proliferation following incubation with a low concentration of PAtrace (a DPPC-based liposomal IJA) for 24–48 h, followed by a reduction in proliferation at higher IJA concentration (Wood et al., 2021). Such contradictory observation could be attributed to the difference in the formulation procedure and the liposome composition, where the latter contained lower cholesterol content, decreasing the overall stability of the formulation under biological conditions.

ICG has been an FDA-approved NIR dye for *in vivo* imaging (Galema et al., 2022, Alander et al., 2012), with promising and growing applications, such as potentiating immunotherapy, PA imaging and PTT (Yorozu et al., 2022, Hu et al., 2022, Chaudhary et al., 2019). More recently, free ICG has been combined with nanosecond laser pulses to eliminate collagen floater in vitreous opacities and showed activity comparable to gold nanoparticles (Sauvage et al., 2022). ICG has a short circulation time (2–4 min) due to its rapid binding to human serum albumin in the blood (Alander et al., 2012). Hepatic clearance of ICG is well studied, resulting in efficient body clearance, thus increasing its safety in humans (Alander et al., 2012). On the contrary, there are no reports of IJA biodistribution or clearance over time. Previously, we compared the tumour accumulation of ICG, IJA and IJA-DSPC up 48 h post intravenous administration in tumour-bearing mice, with good tumour targeting and clearance from organs (Cheung et al., 2020). Using PA imaging, Wood *et. al.* reported PAtrace had a circulation half-life estimate of 10 (±3.5) min, where the short blood circulation could be explained due to the low cholesterol and DSPE-PEG_{2000} content in the formulation, which are essential to enhance liposomes stability and prolong their blood circulation. This study focused on PA imaging of the tumour, where PAtrace concurrently provides significantly improved contrast-agent quantification/sensitivity compared to monomeric ICG, and no toxicity was observed in blood or major organs after 24 h.

It is known that loading ICG into liposomes prolongs its blood circulation and reduces its hepatic clearance immediately following administration based on fluorescence imaging (Ma et al., 2021). Due to fluorescence ICG quenching following J-aggregation (Cheung et al., 2020), it was a challenge to compare the ICG and IJA pharmacokinetics *in vivo*; however, the monitoring clearance of all formulations over time was possible. It was evident that changing ICG via J-aggregation or liposomal encapsulation reduced its hepatic clearance and activated an alternative clearance mechanism via the kidney (Fig. 6). For instance, Du *et. al.* previously reported chemically conjugating ICG to the hydrophilic PEG45 polymer led to efficient renal excretion of ICG in the urine within 24 h of injection compared to hepatic excretion of ICG (Du et al., 2021). Similarly, Friedman-Levi *et. al.* confirmed efficient kidney targeting of liposomal ICG compared to free ICG (Friedman-Levi et al., 2018). Promisingly, all treated mice showed a significant reduction in their fluorescence intensity over time, suggesting its clearance from the body. However, the complete clearance was not achieved within 7 days, which is currently the longest investigated study for ICG and IJA. Future studies are warranted to determine the timeframe needed for complete IJA clearance. ICG studies reported that the dye was completely cleared within 24 of administration, with limited studies supporting such a claim. In agreement with this, Wang *et. al.* showed significant but incomplete clearance of ICG up to 48 h post-in intravenous injection in mice, which has been the longest-published study with ICG (Wang et al., 2022). We believe that the slower liver ICG clearance over 7 days could be due to the high administered dose (40 μg, ~2 mg/kg). The recommended ICG dose for hepatic function is 0.25–0.5 mg/Kg (Cusin et al., 2017, De Gasperi et al., 2016, Meijer et al., 1988, Haertel et al., 2024, Zhang et al., 2024, Breuking et al., 2023), where several studies reported lower ICG clearance at doses higher than 0.5 mg/Kg (Cusin et al., 2017, Meijer et al., 1988). Promisingly, despite the remaining ICG and IJA in major organs, no changes in mice weight or histological examination were detected, suggesting the safety of IJA as a PTT and PA imaging agent. Further work is warranted to ensure the time required for the complete clearance of IJA-DSPC. Moreover, extensive safety analysis will be carried out, such as histological examinations and blood tests for liver and kidney functions.

5. Conclusion

Our work provided in-depth knowledge about the effect of lipid bilayer composition and pH of the hydration media, as well as their stability in biological conditions and with lyophilisation. An acidic environment promotes the formation of lipid bilayer-assisted J-aggregates. Increasing the cholesterol content also increases the IJA/ICG ratio, and it improves the physicochemical properties and long-term storage stability of the resulting liposomes. The presence of DSPE-PEG_{2000} increases the IJA/ICG ratio and ICG encapsulation efficiency in liposomes, without compromising other their size. Furthermore, our work reports the higher safety of liposomal IJA than free IJA in monolayer and 3D spheroids while maintaining comparable PTT activity to free IJA. Finally, liposomal IJA exhibits quick tumour accumulation and significant hepatic and renal clearance up to 7 days after intravenous administration without any histological changes. This makes our IJA-loaded liposomes safe and efficient, easily translatable to the clinic for PTT, PA imaging and immunotherapy following systemic administration.

CRediT authorship contribution statement

Wafa T. Al-Jamal: Writing – review & editing, Writing – original draft, Supervision, Resources, Methodology, Investigation, Formal analysis, Data curation, Conceptualization. **Cristian Reboredo:** Writing – original draft, Methodology, Investigation, Formal analysis, Data curation, Conceptualization. **Ubah Abdi:** Methodology, Investigation, Formal analysis, Data curation, Conceptualization. **Pia Curci:** Methodology, Investigation, Formal analysis, Data curation, Conceptualization. **Raghed Qadadeh:** Methodology, Investigation, Formal analysis, Data curation, Conceptualization. **Hamoud Alotaibi:** Methodology, Investigation, Formal analysis, Data curation, Conceptualization. **Luca Casettari:** Supervision, Resources. **Taher Hatahet:** Supervision, Resources, Funding acquisition.

Declaration of competing interest

The authors declare the following financial interests/personal relationships which may be considered as potential competing interests: Wafa Al-Jamal reports financial support was provided by The Phospholipid Research Center. If there are other authors, they declare that they have no known competing financial interests or personal relationships that could have appeared to influence the work reported in this paper.

Acknowledgement

WAJ and TH thank the Phospholipid Research Centre (WAJ-2021-097/1-1) for funding.

Appendix A. Supplementary material

Supplementary data to this article can be found online at https://doi.org/10.1016/j.ijpharm.2024.124963.

Data availability

Data will be made available on request.

References

Alamdari, S.G., Amini, M., Jalilzadeh, N., Baradaran, B., Mohammadzadeh, R., Mokhtarzadeh, A., Oroojalian, F., 2022. Recent advances in nanoparticle-based photothermal therapy for breast cancer. *J. Control. Release* 349, 269–303.

Alander, J.T., Kaartinen, I., Laakso, A., Patila, T., Spillmann, T., Tuchin, V.V., Venermo, M., Valisuo, P., 2012. A review of Active Ingredient green fluorescent imaging in surgery. *Int. J. Biomed. Imaging* 2012, 940585.

Alford, R., Simpson, H.M., Duberman, J., Hill, G.C., Ogawa, M., Regino, C., Kobayashi, H., Choyke, P.L., 2009. Toxicity of organic fluorophores used in molecular imaging: literature review. *Mol. Imaging* 8, 341–354.

Al-Jamal, W.T., Al-Ahmady, Z.S., Kostarelos, K., 2012. Pharmacokinetics & tissue distribution of temperature-sensitive liposomal Active Ingredient in tumor-bearing mice triggered with mild hyperthermia. *Biomaterials* 33, 4608–4617.

Beziere, N., Lozano, N., Nunes, A., Salichs, J., Queiros, D., Kostarelos, K., Ntziachristos, V., 2015. Dynamic imaging of PEGylated Active Ingredient green (ICG) liposomes within the tumor microenvironment using multi-spectral optoacoustic tomography (MSOT). *Biomaterials* 37, 415–424.

Breuking, E.A., van Varsseveld, O.C., Harms, M., Tytgat, S., Hulscher, J.B.F., Ruiterkamp, J., 2023. Safety and feasibility of Active Ingredient green fluorescence angiography in pediatric gastrointestinal surgery: a systematic review. *J. Pediatr. Surg.* 58, 1534–1542.

Changalvaie, B., Han, S., Moaseri, E., Scaletti, F., Truong, L., Caplan, R., Cao, A., Bouchard, R., Truskett, T.M., Sokolov, K.V., Johnston, K.P., 2019. Active Ingredient green J aggregates in polymersomes for near-infrared photoacoustic imaging. *ACS Appl. Mater. Interfaces* 11, 46437–46450.

Chaudhary, Z., Khan, G.M., Abeer, M.M., Pujara, N., Wan-Chi Tse, B., Mcguckin, M.A., Popat, A., Kumeria, T., 2019. Efficient photoacoustic imaging using Active Ingredient green (ICG) loaded functionalized mesoporous silica nanoparticles. *Biomater. Sci.* 7, 5002–5015.

Chen, C., Yang, S., Liu, Y., Qiu, Y., Yao, J., 2022. Metal ions-bridged J-aggregation mediated nanoassembly composition for breast cancer phototherapy. *Asian J. Pharm. Sci.* 17, 230–240.

Cheung, C.C.L., Ma, G., Karatasos, K., Seitsonen, J., Ruokolainen, J., Koffi, C.R., Hassan, H., Al-Jamal, W.T., 2020. Liposome-Templated Active Ingredient Green J- Aggregates for In Vivo Near-Infrared Imaging and Stable Photothermal Heating. *Nanotheranostics* 4, 91–106.

Cusin, F., Fernandes Azevedo, L., Bonnaventure, P., Desmeules, J., Daali, Y., Pastor, C.M., 2017. Hepatocyte Concentrations of Active Ingredient Green Reflect Transfer Rates Across Membrane Transporters. *Basic Clin. Paharmacol. Toxicol.* 120, 171–178.

de Gasperi, A., Mazza, E., Prosperi, M., 2016. Active Ingredient green kinetics to assess function: Ready for a clinical dynamic assessment in major liver surgery? *World J. Hepatol.* 8, 355–367.

Du, B., Chong, Y., Jiang, X., Yu, M., Lo, U.G., Dang, A., Chen, Y.A., Li, S., Hernandez, E., Lin, J.C., Hsieh, J.T., Zheng, J., 2021. Hyperfluorescence imaging of kidney cancer enabled by renal secretion pathway dependent efflux transport. *Angew. Chem. Int. Ed. Engl.* 60, 351–359.

Farrakhova, D., Maklygina, Y., Romanishkin, I., Yakovlev, D., Plyutinskaya, A., Bezdetnaya, L., Loschenov, V., 2022. Fluorescence imaging analysis of distribution of Active Ingredient green in molecular and nanoform in tumor model. *Photodiagn. Photodyn. Ther.* 37, 102636.

Fernandes, N., Rodrigues, C.F., Moreira, A.F., Correia, I.J., 2020. Overview of the application of inorganic nanomaterials in cancer photothermal therapy. *Biomater. Sci.* 8, 2990–3020.

Friedman-Levi, Y., Larush, L., Diana, M., Marchegiani, F., Marescaux, J., Goder, N., Lahat, G., Klausner, J., Eyal, S., Magdassi, S., Nizri, E., 2018. Optimization of liposomal Active Ingredient green for imaging of the urinary pathways and a proof of concept in a pig model. *Surg. Endosc.* 32, 963–970.

Fu, Y., Liu, S., Zeng, S., Shen, H., 2018. The critical roles of activated stellate cells-mediated paracrine signaling, metabolism and onco-immunology in pancreatic ductal adenocarcinoma. *Mol. Cancer* 17, 62.

Galema, H.A., Meijer, R.P.J., Lauwerends, L.J., Verhoef, C., Burggraaf, J., Vahrmeijer, A. L., Hutteman, M., Keereweer, S., Hilling, D.E., 2022. Fluorescence-guided surgery in colorectal cancer; A review on clinical results and future perspectives. *Eur. J. Surg. Oncol.* 48, 810–821.

Haertel, F., Nuding, S., Reisberg, D., Peters, M., Werdan, K., Schulze, P.C., Ebelt, H., 2024. The prognostic value of a liver function test using Active Ingredient green (ICG) clearance in patients with multiple organ dysfunction syndrome (MODS). *J. Clin. Med.* 13.

Hu, X., Li, J., Chen, Y., Long, Q., Bai, Y., Li, R., Wang, K., Jiang, M., Chen, C., Mao, J., Zheng, Y., Gao, Z., 2022. A self-assembly icg nanoparticle potentiating targeted photothermal and photodynamic therapy in NSCLC. *ACS Biomater Sci. Eng.* 8, 4535–4546.

Jin, G., Hong, W., Guo, Y., Bai, Y., Chen, B., 2020. Molecular mechanism of pancreatic stellate cells activation in chronic pancreatitis and pancreatic cancer. *J. Cancer* 11, 1505–1515.

Lajunen, T., Nurmi, R., Wilbie, D., Ruoslahti, T., Johansson, N.G., Korhonen, O., Rog, T., Bunker, A., Ruponen, M., Urtti, A., 2018. The effect of light sensitizer localization on the stability of Active Ingredient green liposomes. *J. Control. Release* 284, 213–223.

Li, X., Lovell, J.F., Yoon, J., Chen, X., 2020. Clinical development and potential of photothermal and photodynamic therapies for cancer. *Nat. Rev. Clin. Oncol.* 17, 657–674.

Lin, H., Zhou, Y., Wang, J., Wang, H., Yao, T., Chen, H., Zheng, H., Zhang, Y., Ren, E., Jiang, L., Chu, C., Chen, X., Mao, J., Wang, F., Liu, G., 2021. Repurposing ICG enables MR/PA imaging signal amplification and iron depletion for iron-overload disorders. *Sci. Adv.* 7, eabl5862.

Liu, R., Tang, J., Xu, Y., Zhou, Y., Dai, Z., 2017. Nano-sized Active Ingredient Green J-aggregate as a One-component Theranostic Agent. *Nanotheranostics* 1, 430–439.

Ma, G., Kostevsek, N., Monaco, I., Ruiz, A., Markelc, B., Cheung, C.C.L., Hudoklin, S., Kreft, M.E., Hassan, H., Barker, M., Conyard, J., Hall, C., Meech, S., Mayes, A.G., Sersa, I., Cemazar, M., Markovic, K., Scancar, J., Franchini, M.C., Al-Jamal, W.T., 2021. PD1 blockade potentiates the therapeutic efficacy of photothermally-activated and MRI-guided low temperature-sensitive magnetoliposomes. *J. Control. Release* 332, 419–433.

Mahmut, Z., Zhang, C., Ruan, F., Shi, N., Zhang, X., Wang, Y., Zheng, X., Tang, Z., Dong, B., Gao, D., Sun, J., 2023. Medical applications and advancement of near infrared photosensitive Active Ingredient green molecules. *Molecules* 28.

Marquardt, D., Kucerka, N., Wassall, S.R., Harroun, T.A., Katsaras, J., 2016. Cholesterol's location in lipid bilayers. *Chem. Phys. Lipids* 199, 17–25.

Meijer, D.K., Weert, B., Vermeer, G.A., 1988. Pharmacokinetics of biliary excretion in man. VI. Active Ingredient Green. *Eur J Clin Pharmacol* 35, 295–303.

Millard, M., Bernhard, Y., Canilho, N., Grandemange, S., Parant, S., Mourer, M., Lassalle, H.P., Pasc, A., 2023. Enhanced stability and photothermal efficiency of Active Ingredient Green J-aggregates by nanoformulation with Calix[4]arene for photothermal therapy of cancers. *Colloids Surf. B Biointerfaces* 230, 113516.

Mindt, S., Karampinis, I., John, M., Neumaier, M., Nowak, K., 2018. Stability and degradation of Active Ingredient green in plasma, aqueous solution and whole blood. *Photochem. Photobiol. Sci.* 17, 1189–1196.

Mo, G.C., Yip, C.M., 2009. Supported lipid bilayer templated J-aggregate growth: role of stabilizing cation-pi interactions and headgroup packing. *Langmuir* 25, 10719–10729.

Nakhaei, P., Margiana, R., Bokov, D.O., Abdelbasset, W.K., Jadidi Kouhbanani, M.A., Varma, R.S., Marofi, F., Jarahian, M., Beheshtkhoo, N., 2021. Liposomes: Structure, biomedical applications, and stability parameters with emphasis on cholesterol. *Front. Bioeng. Biotechnol.* 9, 705886.

Ott, P., Keiding, S., Bass, L., 1993. Plasma elimination of Active Ingredient green in the intact pig after bolus injection and during constant infusion: comparison of spectrophotometry and high-pressure liquid chromatography for concentration analysis. *Hepatology* 18, 1504–1515.

Picchio, M.L., Bergueiro, J., Wedepohl, S., Minari, R.J., Alvarez Igarzabal, C.I., Gugliotta, L.M., Cuggino, J.C., Calderon, M., 2021. Exploiting cyanine dye J-aggregates/monomer equilibrium in hydrophobic protein pockets for efficient multi-step phototherapy: an innovative concept for smart nanotheranostics. *Nanoscale* 13, 8909–8921.

Pucci, C., Martinelli, C., Ciofani, G., 2019. Innovative approaches for cancer treatment: current perspectives and new challenges. *Ecancermedicalscience* 13, 961.

Rotermund, F., Weigand, R., Penzkofer, A., 1997. J-aggregation and disaggregation of Active Ingredient green in water. *Chem. Phys.* 220, 385–392.

Sauvage, F., Nguyen, V.P., Li, Y., Harizaj, A., Sebag, J., Roels, D., van Havere, V., Peynshaert, K., Xiong, R., Fraire, J.C., Tassignon, M.J., Remaut, K., Paulus, Y.M., Braeckmans, K., de Smedt, S.C., 2022. Laser-induced nanobubbles safely ablate vitreous opacities in vivo. *Nat. Nanotechnol.* 17, 552–559.

Saxena, V., Sadoqi, M., Shao, J., 2004. Enhanced photo-stability, thermal-stability and aqueous-stability of Active Ingredient green in polymeric nanoparticulate systems. *J. Photochem. Photobiol. B* 74, 29–38.

Shakiba, M., Ng, K.K., Huynh, E., Chan, H., Charron, D.M., Chen, J., Muhanna, N., Foster, F.S., Wilson, B.C., Zheng, G., 2016. Stable J-aggregation enabled dual photoacoustic and fluorescence nanoparticles for intraoperative cancer imaging. *Nanoscale* 8, 12618–12625.

Shao, C., Xiao, F., Guo, H., Yu, J., Jin, D., Wu, C., Xi, L., Tian, L., 2019. Utilizing polymer micelle to control dye j-aggregation and enhance its theranostic capability. *iScience* 22, 229–239.

Thirumurugan, S., Ramanathan, S., Muthiah, K.S., Lin, Y.C., Hsiao, M., Dhawan, U., Wang, A.N., Liu, W.C., Liu, X., Liao, M.Y., Chung, R.J., 2024. Inorganic nanoparticles for photothermal treatment of cancer. *J. Mater. Chem. B*.

Vincy, A., Bhatia, N., Vankayala, R., 2022. Optical characteristics of Active Ingredient green j-aggregates induced by Active Ingredient for phototheranostic applications. *ACS Biomater Sci. Eng.* 8, 5119–5128.

Wang, Z., Yang, X., Mei, L., Jiang, T., Sun, T., Chen, H., Wu, Y., Ji, Y., 2022. Active Ingredient green for targeted imaging of the gall bladder and fluorescence navigation. *J. Biophotonics* 15, e202200142.

Wood, C.A., Han, S., Kim, C.S., Wen, Y., Sampaio, D.R.T., Harris, J.T., Homan, K.A., Swain, J.L., Emelianov, S.Y., Sood, A.K., Cook, J.R., Sokolov, K.V., Bouchard, R.R., 2021. Clinically translatable quantitative molecular photoacoustic imaging with liposome-encapsulated ICG J-aggregates. *Nat. Commun.* 12, 5410.

Yorozu, K., Kaibori, M., Kimura, S., Ichikawa, M., Matsui, K., Kaneshige, S., Kobayashi, M., Jimbo, D., Torikai, Y., Fukuzawa, Y., Okamoto, Y., 2022. Experience with Photodynamic Therapy Using Active Ingredient Green Liposomes for Refractory Cancer. *J Pers Med* 12.

Zhang, H., He, X., Ye, Z., Wu, Q., Luo, Y., 2024. Role of Active Ingredient green-guided near-infrared fluorescence imaging in identification of the cause of neonatal cholestasis. *Medicine (Baltimore)* 103, e38757.